

COMPREHENSIVE INVESTIGATION OF PHASE FORMATION MECHANISM AND PHYSICO-MECHANICAL PROPERTIES OF Ca-Mg-SILICATE

Myat Myat-Htun¹, Hossein Mohammadi¹, Ahmad-Fauzi Mohd Noor¹, Masakazu Kawashita², and Yanny Marliana Baba Ismail^{1,*}

¹Biomaterials Niche Group, School of Materials and Mineral Resources Engineering, Engineering Campus, Universiti Sains Malaysia, Pulau Penang, Malaysia, Tel.: +60 45996154, e-mail: yannymarliana@usm.my, srafauzi@usm.my

²Department of Inorganic Biomaterials, Institute of Biomaterials and Bioengineering, Tokyo Medical and Dental University, Tokyo, Japan

Received Date: November 26, 2019; Revised Date: September 20, 2020; Acceptance Date: November 4, 2020

Abstract

This study aimed to investigate extensively the full phase formation mechanism from the lowest temperature to form the phases to the optimum temperature to crystallize akermanite. The effects of various milling speeds and sintering temperatures on physico-mechanical properties of akermanite prepared using high-energy planetary milling method were also investigated. The minimum formation temperature of akermanite phase (above 800°C) was determined by X-Ray diffraction (XRD) and differential thermal analysis. XRD analysis revealed akermanite had formed through gradual phase development with the increase in temperature. Below 700°C, akermanite was structurally unstable while multiple transient compounds (low clinoenstatite, wollastonite, monticellite, and diopside) coexisted, as indicated by low peak intensities. Single phase akermanite was obtained by heat-treating at 1100°C. Physical studies suggested the densest akermanite ceramic feature, with tensile strength range of 25.26 ± 1.41 MPa– 32.10 ± 2.13 MPa and Vickers microhardness range of 1.39 ± 0.04 GPa– 4.94 ± 0.26 GPa could be obtained at 1250°C.

Keywords: Akermanite, High-energy planetary milling, Milling speed, Phase formation mechanism, Sintering temperature

Introduction

Biomedical implants for successful bone repair demand high mechanical strength and fracture toughness with good biological properties. Reviewing the literature on *in vitro* and *in vivo* tests' outcomes [1,2], the formation of hydroxyapatite on implant surface stands as a stringent marker for biological response. Thus, phosphate bioceramics such as hydroxyapatite and tricalcium phosphate-based materials have been widely investigated in the field of bone regeneration due to their good bioactivity, biocompatibility and osteointegration [3]. In the last decade, researchers have identified another important group of bioceramics based on the CaO–MgO–SiO₂ system [4]. Among the materials in this system, akermanite (Ca₂MgSi₂O₇), an alkaline-based melilite-type biosilicate has garnered considerable interest in biomedical applications. This was attributed to the dual angiogenesis/osteogenesis stimulation, controllable biodegradability, cytocompatibility, as well as bone-like apatite formation capability [5]. Studies on cell proliferation of mouse fibroblast L929 cell line showed that alkaline metal ions Ca, Mg and Si released from akermanite degradation notably stimulated the cell proliferation [6]. Additionally, akermanite possessed superior mechanical properties to those of stoichiometric hydroxyapatite (HA), beta-tricalcium phosphate (β-TCP) and bioglass [7].

Several known approaches in synthesizing calcium silicate bioceramics have been reported including sol-gel, chemical precipitation, hydrothermal, and solid-state reaction methods [4]. High-energy mechanical activation is one of the solid-state reaction methods that had been utilized as a processing technique due to its simplicity of experiment, low production cost and rapid synthesis of the product. This technique can produce powders and composites with reduced particle size, thus could enhance the thermodynamic and kinetic reactions between the starting materials [8].

Shamoradi et al. published a study of monticellite-akermanite nanocomposite phase formation by fabricating through mechanical activation [9]. The starting reactants (talc, magnesium carbonate and calcium carbonate) were milled at different ball-milling times 10 min, 2 h, 5 h, 10 h and 20 h. Then, the resultant specimens were sintered at 1200°C for 1 h. Even though the pre-determined composite was successfully prepared, one issue is still needed to be considered in their phase formation analysis. They reported the Gibbs free energy (ΔG) values at 1200°C for all phase formation reactions, including the decomposition reactions of carbonates during milling which generally happens between 600 and 800°C [10]. Their attempt on calculation raises questions regarding actual phase formation energy of reaction. To avoid such confusion, the Gibbs energy for each reaction is reported at specific heat treatment temperature starting from the low temperature in the current study.

To the authors' best knowledge, no single study exists as yet to study the complete akermanite phase formation from a very low temperature to a high temperature via high-energy wet mechanical activation method using different milling speeds, although reviews suggest researchers did investigate phase formation at different various temperatures [11]. The phase development of akermanite heat-treated from a low temperature of 250°C to high temperatures was studied using differential thermal analysis and X-ray diffraction. Comparative studies on morphological, physical, and mechanical characteristics were carried out at different milling speeds and temperatures.

Experimental Procedures

Sample Preparation

Calcium oxide (reagent grade, Sigma-Aldrich, USA), magnesium oxide (99%, Alfa Aesar, USA), and silicon dioxide (99%, Sigma-Aldrich, USA) were milled with a molar ratio of 2:1:2 in a zirconia jar containing zirconia balls in a planetary ball mill (PM 100, Retsch GmbH, Germany). The ball-to-powder weight ratio of 10:1 was employed under air milling atmosphere. Deionized water was used as suspension media. The milling was performed using rotational speeds of 300, 400 and 500 rpm, and the milling time was fixed at 4 h. The resultant slurry was then oven dried at 100°C for 24 h. The dried cake was then ground and sieved using a 200 μm sieve. The resultant powders were then pelletized in an evacuated stainless steel die under 150 MPa pressure forming 13 mm diameter and 3 mm thickness disc-shaped green bodies. The green pellets were then heat-treated at 250, 400, 600, 700, 800, 950, 1100, 1150, 1200, 1250 and 1300°C for 3 h in air atmosphere. The temperatures chosen were based on DTA analysis as well as an attempt to optimize phase formation of akermanite.

Material Characterizations

In an attempt to investigate phases formed in CaO–MgO–SiO₂ system, differential thermal analysis (DTA) and X-ray diffraction (XRD) analyses were conducted. DTA (Setaram Setsys Evolution, France) was performed on the as-milled powders by varying the

temperature from ambient to 1200°C at a heating rate of 10°C/min in air atmosphere. XRD (D2 Phaser, Bruker AXS Inc., USA) with monochromatic Cu-K α radiation ($\lambda = 0.154$ nm) was used to determine the phases formed in the 2θ range of 10° to 80° with a scan step of 0.05° and 1.25 sec counting time from very low temperature (250°C) to high temperature. The crystallite size was estimated applying Scherrer's Equation [12].

Morphological observation of the as-milled powders and the sintered akermanite ceramics was performed using field emission scanning electron microscope (FESEM; Zeiss Supra™ Gemini 35 VP, Germany).

Relative density of the sintered bodies was determined in accordance with ASTM B962-17 [13] by applying Archimedes' principles. Diametral tensile strength (DTS) test was also conducted on the sintered pellets, and positioned vertically using a universal testing machine (Instron 3369, Illinois Tool Works Inc., UK) with a loading rate of 0.5 mm/min, in accordance with ASTM D3967-95a [14].

Vickers microhardness (H_v) was performed on polished sintered pellets in accordance with ASTM E384-99 procedure [15] using a digital Vickers microhardness tester (FV-810, Future-Tech Corp., Japan) with a diamond pyramid indenter, at 5 kilograms-force (kg.f) load for dwelling time of 10 secs at room temperature. Fracture toughness (K_{IC}) was estimated by taking the average of all crack lengths produced for each indentation as stated by Avans and Charles [16].

$$K_{IC} = 0.0824 \frac{F}{C^{3/2}} \quad (1)$$

where, F is the applied load (N), and C is radial crack length (m) measured from the center point of the indented area.

Assessment of specific surface area of as-milled powders was conducted by N₂ adsorption (ASAP™ 2020 Plus, Micromeritics Instrument Corp., USA) adopting Brunauer–Emmett-Teller (BET) method [12].

Results and Discussion

Thermal Analysis

A complete phase formation mechanism was studied from thermal analysis of the as-milled powders. According to the DTA analysis, as-milled powders were heat-treated at various temperatures and subsequently XRD analysis was conducted to determine the formation mechanism of different phases.

The DTA curve (Figure 1) of as-milled powder heat-treated to 1200°C exhibits three endothermic peaks and one exothermic peak. The first endothermic peak between 250 and 400°C is associated to enstatite formation [17], whereas the second peak between 400 and 600°C can be ascribed as the development of diopside phase. The third endothermic peak (600 to 800°C) is believed to be formation of merwinite. The narrow exothermic peak between 800 and 950°C is assumed to be the phase formation of crystalline akermanite structure. This analysis will be confirmed with XRD, whereby pellets were prepared separately, and subsequently heat-treated at the temperatures selected (250, 400, 600, 700, 800, 950, 1100, 1150, 1200, 1250, 1300°C) in accordance to the DTA curve.

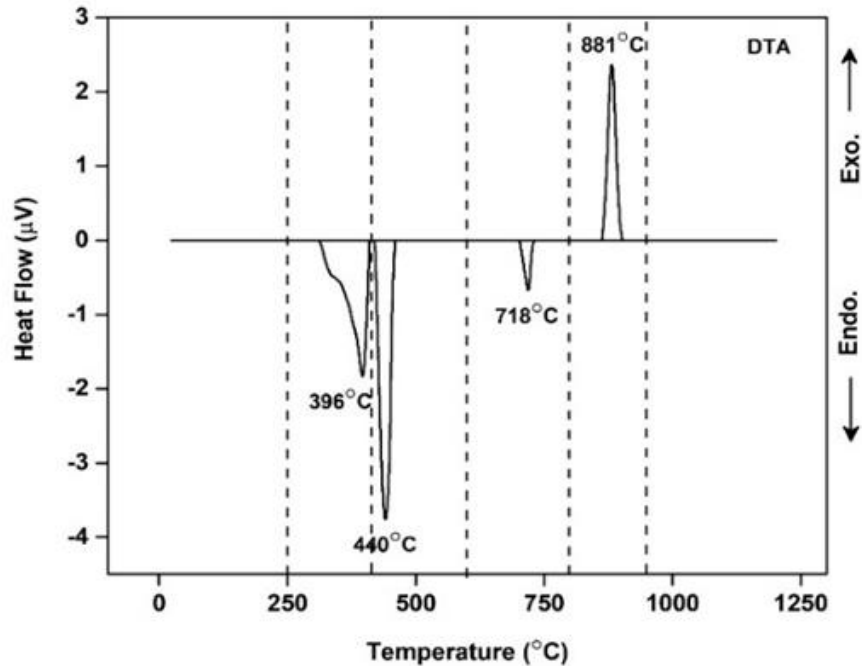


Figure 1. DTA curve of as-milled powder heat-treated at different temperatures

Phase Analysis

Figure 2 depicts the XRD patterns of as-milled and heat-treated powders produced using high-energy planetary mill at 300, 400 and 500 rpm for 4 h under the same preparation condition. The XRD profiles of as-milled powders were observed with sharp features, revealing crystalline structured phase. The crystallite sizes were calculated to be in the range 45.5 to 43.3 nm when the milling speed was increased from 300 to 500 rpm. Referring to Figure 2 (a1, a2), the as-milled powders (500 rpm milling speed) showed the formation of new transient phases of low clinoenstatite (MgSiO_3 ; ICSD card no. 98-011-0759), wollastonite (CaSiO_3 ; ICSD card no. 98-001-7684), and monticellite (CaMgSiO_4 ; ICSD card no. 98-004-5808), besides unreacted lime (CaO ; ICSD card no. 98-003-4917), periclase (MgO ; ICSD card no. 98-011-0579), and low quartz (SiO_2 ; ICSD card no. 98-001-2528). The formations of wollastonite and monticellite at low temperature upon milling have never been reported elsewhere in the literature. Our findings also highlighted that akermanite phase could not be formed by intense high-speed milling, suggesting heat treatment is required.

CaO and MgO would react with SiO_2 to form low clinoenstatite (MgSiO_3) and wollastonite (CaSiO_3) at 200°C and 300°C , respectively [17,18]. In the synthesis of akermanite, the formation of MgSiO_3 and CaSiO_3 was possible as the temperature in the planetary mill can reach to a temperature range of $200\text{--}600^\circ\text{C}$ [19]. Such high temperatures during milling had received relatively little attention so far. The temperature increment and intense mechanical deformation enhanced the diffusivity of reactants and accelerated reaction kinetics, triggering the phase formation behavior of MgSiO_3 and CaSiO_3 [20]. In mineralogy studies, Christie had emphasized the formations of wollastonite and monticellite at minimum temperature 200°C during the low temperature breakdown of the akermanite system under various water pressures [21].

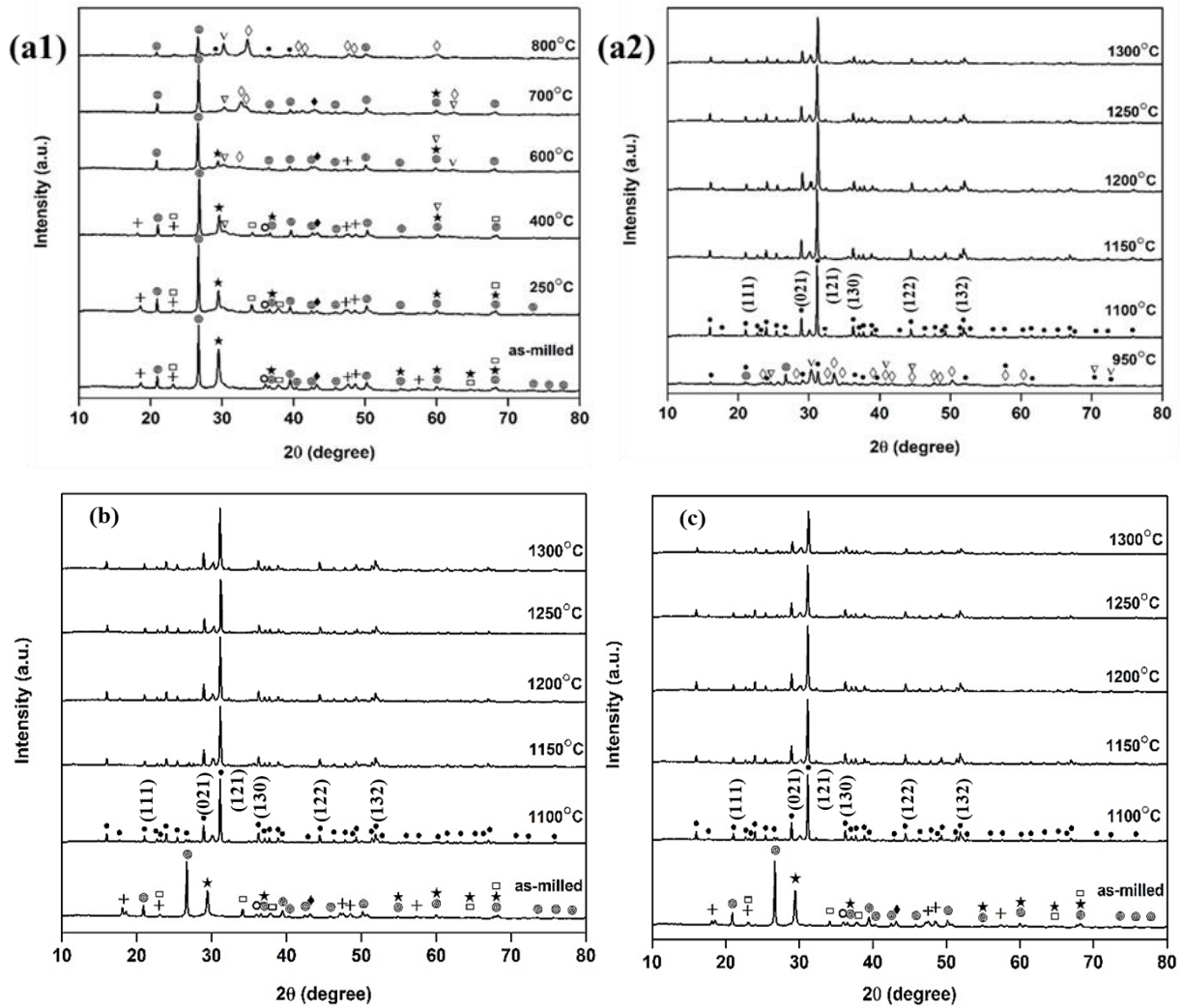


Figure 2. XRD spectra in the range $10^{\circ} - 80^{\circ}$: (a1, a2) 500 rpm, (b) 400 rpm, (c) 300 rpm, and (● : akermanite, ▽ : diopside, ◇ : merwinite, ◎ : low quartz, □ : monticellite, + : wollastonite, ○ : lime, ◆ : periclase, ★ : low clinoenstatite)

Additionally, heat treatment at a low temperature of 250°C confirmed the same phase as as-milled, i.e., low clinoenstatite, wollastonite and monticellite. Hence, the first stage in the akermanite formation process at low temperature can be reported as follows, with ΔG values determined.



Gibbs free energy (ΔG) helps researchers predict the thermodynamic behaviors of chemical changes. In our work, the Gibbs energies for all possible reactions at specified temperature were estimated by adapting the Gibbs' relation [22]. If ΔG value is negative, the reaction is spontaneous (product-favored). If ΔG is positive, the reaction is non-spontaneous (reactant-favored) and if ΔG is zero, the system is in equilibrium. As seen, all the above

reactions and subsequent reactions showed negative ΔG values indicating high tendency to favor the spontaneous formation of desired products from the thermodynamics standpoint.

Upon further heat treatment to a temperature of 400°C, monticellite and periclase peak intensities decreased as the new phase diopside ($\text{CaMgSi}_2\text{O}_6$; ICSD card no. 98-011-0180) started developing with low intensity. Therefore, in the next stage the formation of diopside can be expressed as follows:



Reaction (5) was also similarly reported by Rietmeijer et al. through laboratory condensation experiments of refractory Ca-SiO₂-H₂-O₂ [23]. Further heating to 600°C led to the weakening and elimination of lime, low quartz, low clinoenstatite, wollastonite, and monticellite peaks, while the intensity of the diopside peaks increased. New phase of merwinite ($\text{Ca}_3\text{MgSi}_2\text{O}_8$; ICSD card no. 98-004-8556) with low intensity could also be identified. The formation of merwinite along with the reduction of wollastonite, monticellite as well as periclase occurred through the following reaction.



Yoder outlined the coexistence of diopside and merwinite at minimum temperature of 750°C under CO₂ pressure in his geological studies on melilite-bearing rocks [24]; in our study, in contrast the formation began at 600°C and this is made possible because of the fine powder interaction after milling. Further heating to 700°C resulted in more pronounced merwinite and diopside. By 800°C, the new phase akermanite ($\text{Ca}_2\text{MgSi}_2\text{O}_7$; ICSD card no. 98-002-2319) had begun to form. Heat treatment to 950°C gave rise to the progressive development of akermanite phase. This phenomenon suggests that heat treatment is a key process in forming akermanite phase owing to the improvement of powder reactivity.

A previous study mentioned that akermanite powder sintered at 1100°C through sol-gel process would contain merwinite and diopside phases as impurities [25]. However, in this study, the increase in temperature to 1100°C eliminated the merwinite and diopside phases, and the diffraction peaks were in good agreement with those of akermanite phase. It can be reported that merwinite and diopside reacted with each other to form akermanite phase. Hence, our finding highlighted that the temperature above 800°C is required to initiate the formation of akermanite phase in accordance to equation (7).



The ΔG value obtained for the formation of akermanite was smaller than that of literature data [22]. This is because the smaller ΔG values of complex starting compounds (diopside and merwinite) produced the smaller estimated result of product (akermanite). Knowing that equilibrium lines where $\Delta G = 0$, the smaller ΔG of product, the closer to equilibrium, thus the earlier pure phase formation of akermanite.

At temperatures of 1150, 1200, 1250 and 1300°C, the XRD patterns showed similar peaks as those at 1100°C, indicating the phase stability of pure akermanite above 1100°C. We found lower sintering temperature (1100°C) was needed for pure akermanite fabrication than those prepared by previous researchers [6,26]. The rationalization for this is that high-energy planetary ball-milling had activated more rapidly the surfaces of milled powders forming finer particle size which facilitated the chemical reactions during sintering. Akermanite phase stability between 1100 and 1300°C could also be identified similarly for

milling speeds of 300 and 400 rpm and the corresponding XRD spectra are presented in Figure 2 (b, c). The phase analyses for the different speeds of 300, 400 and 500 rpm will be used to relate to the mechanical studies in the present work. The prominent feature of phase stability of akermanite during sintering over a wide range of temperatures can also be very valuable for other applications with demanding mechanical and thermal requirements as well as luminescence properties activated by doping some rare earth ions (Eu^{2+} , Mn^{2+} , Dy^{3+} , etc.) [26].

Recently, Tavangarian and co-workers studied phase formation for CaO-MgO-SiO_2 system using carbonate-based ingredients (calcium carbonate, magnesium carbonate and silicate) through dry planetary ball-milling for 1 min, 5 h, 10 h, 20 h and 50 h [11]. Subsequent heat treatments were then employed from 700 to 1200°C. No phase formation at low temperatures were investigated in their work. Their results showed mixed of binary compounds (enstatite, wollastonite and larnite) and ternary compounds (merwinite and akermanite) had dominated until 1200°C with 5 h milling. To form single phase, the milling time was further increased to longer times of 10 h, 20 h and 50 h. Although pure akermanite phase was achieved at 900°C after 20 h and 50 h milling, the process was deemed to suffer from techno-economical points due to the prolonged milling time and potentially increased contaminant levels. Furthermore, non-uniformity of mixing resulting from dry milling could occur. Therefore, adopting the high-energy high-impact planetary ball-milling would enable the development of final products with use of less energy and reduce time of production, as well as improve properties of the materials.

Morphological and Physical Evaluations

The manipulation of microstructure is key to control densification and thus, the mechanical properties of materials to be engaged as strength-sufficient bone repair substitutes for clinical purposes. In the present study, to optimise these properties, two parameters were varied: milling speed and sintering temperature.

Figure 3 (a-c) shows the micrographs of powders that were milled at 300, 400 and 500 rpm for 4 h. As observed, the powder morphologies showed increase in degree of agglomeration with milling speed. This phenomenon is reasonably assumed that the smaller the particles, the higher surface energy, thus the greater cohesion between particles and easier for particles to agglomerate [27]. This is consistent with the resultant BET specific surface area increment from 77.79 to 88.51 and 108.68 m^2/g in terms of increasing milling speed.

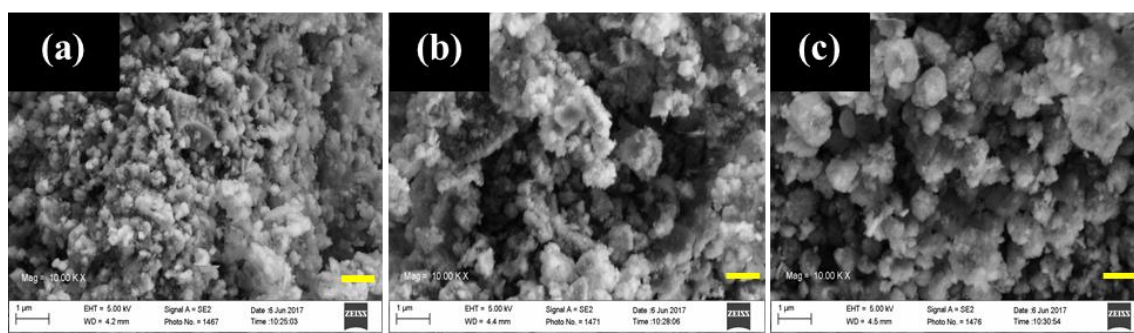


Figure 3. Morphologies of as-milled powders at different milling speeds: (a) 300 rpm, (b) 400 rpm, and (c) 500 rpm (Magnification = 10,000X, Scale bar = 1 μm)

The surface morphologies of sintered pellets revealed irregular grain geometry (Figure 4). Sintering temperature had greater influence on grain growth of $\text{Ca}_2\text{MgSi}_2\text{O}_7$ rather than milling speeds. The grains grew gradually from 1100 to 1200°C along with loose-

packed grain boundaries and significantly high porosities. Despite this, the grain growth increased to a significant level, thus clear, well-defined grain boundaries became pronounced at 1250°C. Hence, the relative density was increased between 1100 and 1250°C as a function of sintering temperatures, but later, a slight decrease at 1300°C (Figure 5). The optimum densification of akermanite ceramics was achieved at 1250°C as this was attributed to some regions where the grains tend to join together, developing into larger grains. One can observe the mixed of larger grains surrounded by smaller ones, thus filling the spaces between the grains and enhancing the density of sintered solid compacts. Such microstructure can possess improved mechanical properties than those of other monolithic ceramics, as previously described by Niihara [28]. It is noteworthy that akermanite specimens partially melt and grains appeared to be elongated, while some trapped pores were also observed, which would have adverse effect of reaching to 1300°C, and consequently, led to decrease in relative density as shown in Figure 5.

The evidences in microstructural and physical studies suggested that, with the rise in sintering temperature until the threshold temperature (1250°C), the changes in grain growth behaviour and grain size arouse an appreciable positive effect on the overall densification in specimens. In this study, much higher levels for densification (93.72–96.83%) were successfully achieved with respect to those reported by Wu and Chang (70.10%) [29]. Hence, tailoring of densification and subsequent improved mechanical properties of the ceramics appeared to be controlled by nano-sized product and appropriate sintering temperature without changing phase composition.

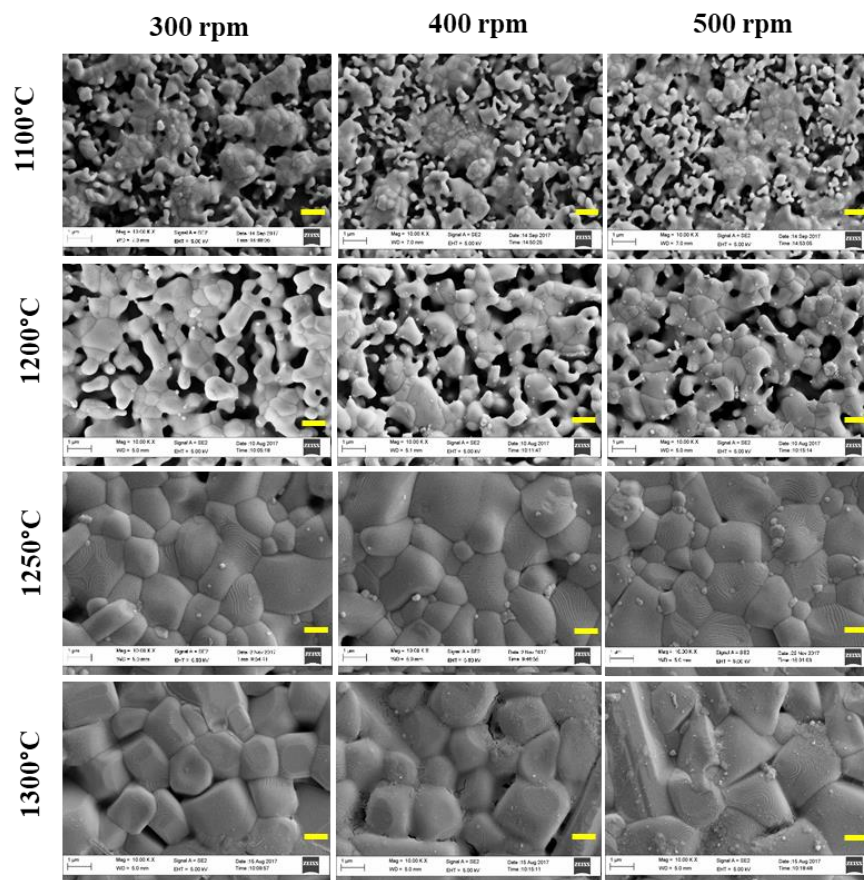


Figure 4. A comparison of FESEM micrographs of outermost surfaces of ceramics (Magnification = 10,000X, Scale bar = 1 µm)

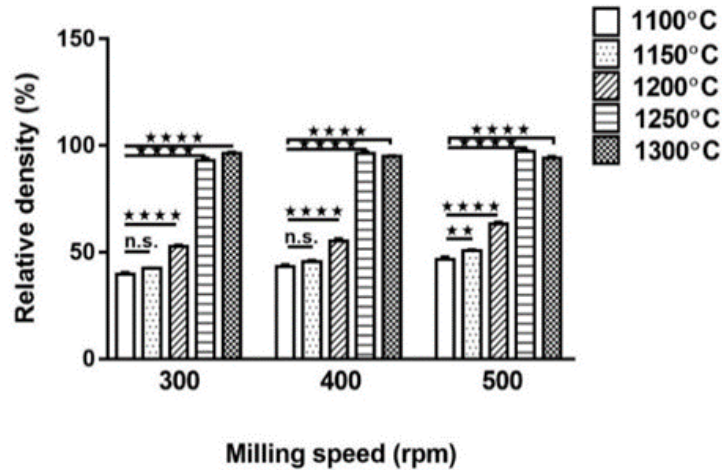


Figure 5. Density of akermanite samples (n.s.: not significant, ****: $p < 0.05$, $n = 5$)

Mechanical Evaluations

Diametral tensile strength, Vickers microhardness and fracture toughness evaluations were conducted to study the influence of sintering temperatures and milling speeds on the mechanical properties of akermanite ceramics. Based on the microstructural and physical results, mechanical tests were performed only on the dense ceramics sintered at 1200 and 1250°C, since higher strength and toughness of material was expected to achieve at these two temperatures, while the akermanite partially melted at 1300°C.

Table 1 demonstrates a clear three- to four-fold increment in DTS values from 1200 to 1250°C, signifying sintering improved the mechanical properties of akermanite. The DTS values achieved at 1200°C were 6.29 ± 0.80 MPa, 8.38 ± 0.89 MPa, and 12.39 ± 1.33 MPa at 300, 400 and 500 rpm, respectively, demonstrating the effect of higher milling speed. The DTS values significantly increased at 1250°C. The low DTS at 1200°C was attributed to its higher residual porosity (Figure 4). DTS of ceramics is considered to be very sensitive to some factors, viz., the presence of flaws (i.e., pore-like and crack-like flaws), grain size and brittle nature of ceramics, based on strength-porosity-microstructure relationships as analyzed by earlier researchers in detail [30]. This porosity dependence of the strength could similarly be found in bone mineral with increasing age [31]. On the whole, all the akermanite samples exhibited higher DTS values than that of HA (4–5 MPa) [32] and β -TCP (~4 MPa) [33]. The highest strength (32.10 ± 2.13 MPa) was achieved by milling at 500 rpm and sintered at 1250°C whilst for that of cancellous bone was 1.5–38 MPa [34]. No other authors have reported such high DTS for dense akermanite ceramics so far, and the high DTS value achieved was attributed to the relatively high density.

Table 1. DTS Values of Sintered Materials (Mean \pm SD, $n = 5$)

Temperature (°C)	DTS \pm SD (MPa)		
	300 rpm	400 rpm	500 rpm
1200	6.29 ± 0.80	8.38 ± 0.89	12.39 ± 1.22
1250	25.26 ± 1.41	27.84 ± 2.27	32.10 ± 2.13

Hardness (H_V) and fracture toughness (K_{IC}) are also important parameters required for the prediction of mechanical performance of bone implants for their potential biomedical applications. The limited strength and fracture toughness have so far hindered the use of bioceramics for stress and load-bearing applications and the enhancement remains a clinical challenge.

To evaluate K_{IC} precisely, the continuous radial cracks emanating from the four vertices and two diagonals of indentation were determined from enlarged FESEM micrographs of gold-coated indented areas, as recommended by Ponton and Rawlings [35]. Typical indented surfaces are presented in Figure 6 (a, b). The measurements were undertaken in the crack-free areas to lessen the influence of thermal cracks on the results.

There was a drastic difference in microhardness behavior between 1200 and 1250°C. The indentation depth and size on sample sintered at 1200°C was deeper and larger than that at 1250°C. This temperature-dependent behavior for microhardness resembles those of densification and degree of crystallization, and concurs well with our initial microstructural analysis (Figure 4). Comparing the H_V results of test samples with previous literature for cancellous bone (0.35 GPa) [36] and natural bone derived hydroxyapatite (0.17–1.47 GPa) [37], generally, higher microhardness was attained in the current prepared samples. Low hardness values (0.86 ± 0.01 GPa) at 1200°C were correlated to the low density (high porosity) of these materials. On the other hand, the compacts sintered at 1250°C possessed improved microhardness (4.94 ± 0.26 GPa) than natural bone extracted materials.

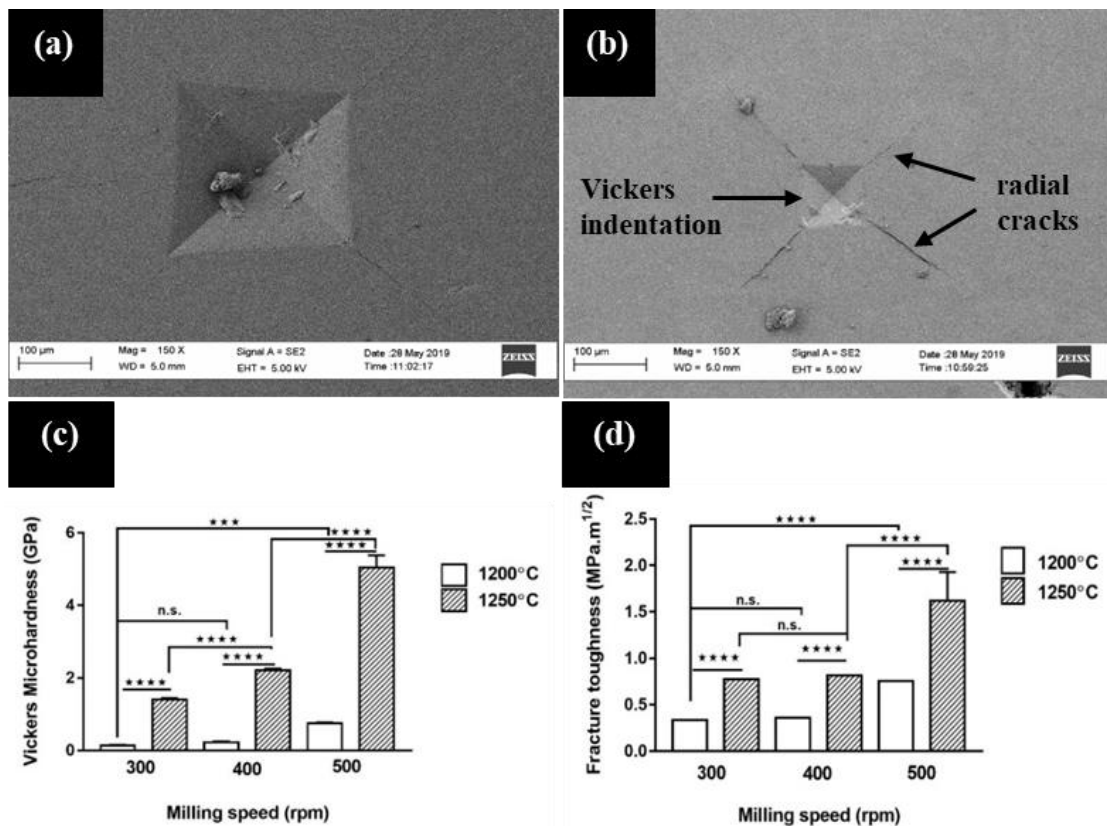


Figure 6. Vickers microhardness indentation marks on polished samples milled with 500 rpm: (a) 1200°C, (b) 1250°C, (c) Vickers microhardness, and (d) fracture toughness (****: $p < 0.05$, one-way ANOVA multiple comparisons' test)

Likewise, fracture toughness of akermanite was increased relatively from $0.34 \pm 0.01 \text{ MPa.m}^{1/2}$ to $0.75 \pm 0.01 \text{ MPa.m}^{1/2}$ with milling speed at 1200°C which was higher than that of the previous work (AK; $0.35 \text{ MPa.m}^{1/2}$) [29]. At 1250°C , fracture toughness presented an improvement from $0.78 \pm 0.01 \text{ MPa.m}^{1/2}$ to $1.62 \pm 0.02 \text{ MPa.m}^{1/2}$, as compared to that of past results (AK; $\sim 1.53 \text{ MPa.m}^{1/2}$) [38], wollastonite (CaSiO_3 ; $< 1.0 \text{ MPa.m}^{1/2}$) [39], HA ($0.70\text{--}0.80 \text{ MPa.m}^{1/2}$) [40], β -TCP ($0.46 \text{ MPa.m}^{1/2}$) [41], bioglass[®]45S5 ($0.70\text{--}1.10 \text{ MPa.m}^{1/2}$) [42] and human cancellous bone ($0.10\text{--}0.80 \text{ MPa.m}^{1/2}$) [39]. The observed low fracture toughness at 1200°C could be interpreted as being a result of weak grain boundaries of akermanite at low temperature. More desirable fracture toughness of akermanite milled with 500 rpm at 1250°C was achieved as close to the range of that for human cortical bone ($2\text{--}12 \text{ MPa.m}^{1/2}$) [39]. Thus, the high value of relative density was in turn a strong reason for high fracture toughness.

It is worth to note that even though we could improve densification and DTS of akermanite bioceramics in the present work, that improvement did not reflect significantly in fracture toughness. One of the possible explanations is the large average grain size of ceramics owing to rapid grain growth at 1250°C , accompanying improved densification. Bower and Ortiz remarked that the apparent change in toughness of ceramics could be affected by the variations in grain size, and it could be improved by designing their microstructure appropriately to achieve refined grain size [43]. Moreover, Ponton and Rawlings outlined that, in brittle polycrystalline materials, the microstructure strongly influenced the indentation cracks such as crack termination at porosity and/or grain boundaries normal to crack path [35]. To address this limitation, further development of better strong and tough materials without losing bioactivity might be possible by substituting metallic ions or compositing with other beneficial second reinforcing phase to impose an effective limit on grain growth of akermanite by reducing the movement of grain boundaries during sintering. The smaller the grains formed, the higher grain boundary surface area and subsequently enhanced mechanical properties since grain boundaries behaved as microstructural barriers to resist micro-crack propagation [44]. Mechanical strength of dense bioceramics fabricated in current work could potentially meet the requirements for bone repair materials.

Conclusions

Akermanite ceramics have been produced by high-energy planetary milling with subsequent heat treatment at 1100°C for 3 h for 300, 400 and 500 rpm. In the present study, formation of both binary phases (CaSiO_3 , MgSiO_3) and ternary phase (CaMgSiO_4) was observed at low temperatures while formation of ternary phases ($\text{Ca}_2\text{MgSiO}_6$, $\text{Ca}_3\text{MgSi}_2\text{O}_8$) developed progressively at high temperature until a pure akermanite was produced. The effects of heat treatment temperatures of akermanite influenced the mechanism of phase formations. Concisely, our findings highlight the appropriate sintering temperature and milling parameters promote the ceramic sinterability, a useful strategy to develop a high-strength $\text{Ca}_2\text{MgSi}_2\text{O}_7$ ceramic with densest characteristics ($> 90\%$) at 1250°C with 500 rpm, which will make akermanite a strong efficient candidate suitable for bone repair applications.

Acknowledgements

The authors acknowledge AUN/SEED-Net and JICA (Grant no. 304.PBAHAN.6050369) and MOHE-FRGS (6071376) for the financial support, as well as Universiti Sains Malaysia and Tohoku University for the facilities.

References

- [1] S.M. Best, A.E. Porter, E.S. Thian, and J. Huang, "Bioceramics: Past, present and for the future," *Journal of European Ceramics Society*, Vol. 28, No.7, pp. 1319-1327, 2008.
- [2] M. Bohner, L. Galea, and N. Doebelin, "Calcium phosphate bone graft substitutes: Failures and hopes," *Journal of European Ceramics Society*, Vol. 32, No. 11, pp. 2663-2671, 2012.
- [3] C. Balázs, F. Wéber, Z. Kövér, E. Horváth, and C. Németh, "Preparation of calcium-phosphate bioceramics from natural resources," *Journal of European Ceramics Society*, Vol. 27, No. 2-3, pp. 1601-1606, 2007.
- [4] C. Wu, and J. Chang, "A review of bioactive silicate ceramics," *Biomedical Materials*, Vol. 8, No. 3, 032001, 2013.
- [5] Y. Huang, X. Jin, X. Zhang, H. Sun, J. Tu, T. Tang, J. Chang, and K. Dai, "In vitro and in vivo evaluation of akermanite bioceramics for bone regeneration," *Biomaterials*, Vol. 30, No. 28, pp. 5041-5048, 2009.
- [6] C. Wu, J. Chang, S. Ni, and J. Wang, "In vitro bioactivity of akermanite ceramics," *Journal of Biomedical Materials Research - Part A*, Vol. 76, No. 1, pp. 73-80, pp. 73-80, 2006.
- [7] C. Shuai, B. Yang, S. Peng, and A. Min, "Improved mechanical properties of beta-tricalcium phosphate by addition of akermanite and 45S5 bioglass," *Materials Research Innovations*, Vol. 18, pp. S2-69-S2-73, 2006.
- [8] H. Barzegar Bafrooei, T. Ebadzadeh, and H. Majidian, "Microwave synthesis and sintering of forsterite nanopowder produced by high energy ball milling," *Ceramics International*, Vol. 40, No. 2, pp. 2869-2876, 2014.
- [9] F. Shamoradi, R. Emadi, and H. Ghomi, "Fabrication of monticellite-akermanite nanocomposite powder for tissue engineering applications," *Journal of Alloys and Compounds*, Vol. 693, pp. 601-605, 2017.
- [10] F. Tavangarian, and R. Emadi, "Mechanism of nanostructure bredigite formation by mechanical activation with thermal treatment," *Materials Letter*, Vol. 65, No. 15-16, pp. 2354-2356, 2011.
- [11] F. Tavangarian, and C.A. Zolko, A. Fahami, A. Forghani, and D. Hayes, "Facile synthesis and structural insight of nanostructure akermanite powder," *Ceramics International*, Vol. 45, No. 6, pp. 7871-7877, 2019.
- [12] I. Cacciotti, A. Bianco, M. Lombardi, and L. Montanaro, "Mg-substituted hydroxyapatite nanopowders: Synthesis, thermal stability and sintering behaviour," *Journal of European Ceramics Society*, Vol. 29, No. 14, pp. 2969-2978, 2009.
- [13] ASTM B962-17, "Standard test methods for density of compacted or sintered powder metallurgy products using Archimedes' principle," *ASTM Int. West Conshohocken, PA*, pp. 1-6, 2010.
- [14] ASTM D3967-95a, "Standard test method for splitting tensile strength of intact rock core specimens," *ASTM Int. West Conshohocken, PA*, pp. 20-23, 2008.
- [15] ASTM E384-99, "Standard test method for microindentation hardness of materials," *ASTM Int. West Conshohocken, PA*, Vol. 14, pp. 1-24, 1999.
- [16] E.A. Charles and A.G. Evans, Fracture toughness determinations by indentation, *Journal of American Ceramics Society*, Vol. 59, pp. 371-372, 1976.
- [17] R. Michel, M.R. Ammar, J. Poirier, and P. Simon, "Phase transformation characterization of olivine subjected to high temperature in air," *Ceramics International*, Vol. 39, No. 5, pp. 5287-5294, 2013.
- [18] W. Mielcarek, D. Nowak-Woźny, and K. Prociów, "Correlation between MgSiO₃ phases and mechanical durability of steatite ceramics," *Journal of European Ceramics Society*, Vol. 24, No. 15-16, pp. 3817-3821, 2004.

- [19] L. Takacs, and J.S. McHenry, "Temperature of the milling balls in shaker and planetary mills," *Journal of Materials Science*, Vol. 41, No. 16, pp. 5246-5249, 2006.
- [20] C. Suryanarayana, "Mechanical alloying and milling mechanical engineering," *Progress in Materials Science*, Vol. 46, No. 1-2, pp. 1-184, 2001.
- [21] O.H.J. Christie, "On Sub-solidus relations of silicates. IV. The systems åkermanite-sodium-gehlenite and gehlenite-sodium-gehlenite," *Norsk geologisk tidsskrift*, Vol. 42, pp. 31-44, 1961.
- [22] R. Li, T. Zhang, Y. Liu, and S. Kuang, "A reaction method for estimating Gibbs energy and enthalpy of formation of complex minerals," *Metallurgical and Materials Transactions B*, Vol. 48, No. 2, pp. 1123-1133, 2017.
- [23] F.J.M. Rietmeijer, A. Pun, Y. Kimura, and J.A. Nuth, "A refractory Ca-SiO-H₂-O₂ vapor condensation experiment with implications for calciosilica dust transforming to silicate and carbonate minerals," *International Journal of Solar System Studies*, Vol. 195, No. 1, pp. 493-503, 2007.
- [24] H.S. Yoder, "Relationship of melilite-bearing rocks to kimberlite: A preliminary report on the system akermanite-CO₂," *Physics and Chemistry of the Earth*, Vol. 9, pp. 883-894, 1975.
- [25] C. Wu, and J. Chang, "Synthesis and apatite-formation ability of akermanite," *Materials Letter*, Vol. 58, No. 19, pp. 2415-2417, 2004.
- [26] E. Karacaoglu, and B. Karasu, "Effect of activators and calcination on luminescence properties of åkermanite type phosphors," *Indian Journal of Chemistry-Section A Inorganic, Physical, Theoretical and Analytical Chemistry*, Vol. 54A, No. 11, pp. 1394-1401, 2005.
- [27] M.S. El-Eskandarany, "Mechanical alloying: Nanotechnology, materials science and powder metallurgy," 1st Edition, William Andrew, Oxford, UK, 2015.
- [28] K. Niihara, "New design concept of structural ceramics: Ceramic nanocomposites," *The Centennial Memorial Issue of The Ceramic Society of Japan*, Vol. 10, pp. 974-982, 1991.
- [29] C. Wu, and J. Chang, "A novel akermanite bioceramic: Preparation and characteristics," *Journal of Biomaterials Applications*, Vol. 21, No. 2, pp. 119-129, 2006.
- [30] E. Martin, D. Leguillon, O. Sevecek, and R. Bermejo, "Understanding the tensile strength of ceramics in the presence of small critical flaws," *Engineering Fracture Mechanics*, Vol. 201, pp. 167-175, 2018.
- [31] X.D. Wang, N.S. Masilamani, J.D. Mabrey, M.E. Alder, and C.M. Agrawal, "Changes in the fracture toughness of bone may not be reflected in its mineral density, porosity, and tensile properties," *Bone*, Vol. 23, No. 1, pp. 67-72, 1998.
- [32] L.T. Bang, K. Ishikawa, and R. Othman, "Effect of silicon and heat-treatment temperature on the morphology and mechanical properties of silicon-substituted hydroxyapatite," *Ceramics International*, Vol. 37, pp. 3637-3642, 2011.
- [33] H. Monma, "Tricalcium phosphate with ceramics complexed hydroxyapatite," *Yogyo-Kyokai-Shi*, Vol. 95, No. 1104, pp. 60-64, 1987.
- [34] S.N. Khan, R.M. Warkhedkar, and A.K. Shyam, "Human bone strength evaluation through different mechanical tests," *Journal of Current Engineering and Technology*, Vol. 2, No. 2, pp. 539-543, 2014.
- [35] C.B. Ponton, and R.D. Rawlings, "Vickers indentation fracture toughness test Part 2 Review of literature and formulation of standardised indentation toughness equations," *Materials Science and Technology*, Vol. 5, No. 10, pp. 865-872, 1989.
- [36] S. Pramanik, A.K. Agarwal, and K.N. Rai, "Development of high strength hydroxyapatite for hard tissue replacement," *Trends in Biomaterials & Artificial Organs*, Vol. 19, No. 1, pp. 46-51, 2005.

- [37] I.P.G. Goller, F.N. Oktar, S. Agathopoulos, D.U. Tulyaganov, J.M.F. Ferreira, and E.S. Kayali, "Effect of sintering temperature on mechanical and microstructural properties of bovine hydroxyapatite (BHA)," *Journal of Sol-Gel Science and Technology*, Vol. 37, No. 2, pp. 111-115, 2006.
- [38] X. Chen, J. Ou, Y. Wei, Z. Huang, Y. Kang, and G. Yin, "Effect of MgO contents on the mechanical properties and biological performances of bioceramics in the MgO–CaO–SiO₂ system," *Journal of Materials Science: Materials in Medicine*, Vol. 21, No. 5, pp. 1463-1471, 2010.
- [39] H. Mohammadi, M. Sepantafar, and A. Ostadrahimi, "The role of bioinorganics in improving the mechanical properties of silicate ceramics as bone regenerative materials," *Journal of Ceramic Science and Technology*, Vol. 6, No. 1, pp. 1-8, 2015.
- [40] P. Van Landuyt, F. Li, J.P. Keustermans, J.M. Streydio, F. Delannay, and E. Munting, "The influence of high sintering temperatures on the mechanical properties of hydroxylapatite," *Journal of Materials Science: Materials in Medicine*, Vol. 6, pp. 8-13, 1995.
- [41] S. Hesarakhi, M. Safari, and M.A. Shokrgozar, "Development of β -tricalcium phosphate/sol-gel derived bioactive glass composites: Physical, mechanical, and in vitro biological evaluations," *Journal of Biomedical Materials Research*, Vol. 91, No. 1, pp. 459-469, 2009.
- [42] L. Gerhardt, and A.R. Boccaccini, "Review-Bioactive glass and glass-ceramic scaffolds for bone tissue engineering," *Materials (Basel)*, Vol. 3, No. 7, pp. 3867-3910, 2010.
- [43] A.F. Bower, and M. Ortiz, "The influence of grain size on the toughness of monolithic ceramics," *Journal of Engineering Materials and Technology*, Vol. 115, No. 3, pp. 228-236, 2008.
- [44] K. Tanaka, Y. Akiniwa, Y. Nakai, and R.P. Wei, "Modelling of small fatigue crack growth interacting with grain boundary," *Engineering Fracture Mechanics*, Vol. 24, No. 6, pp. 803-819, 1986.